Original Research

Transperineal Prostate Biopsy Under Magnetic Resonance Image Guidance: A Needle Placement Accuracy Study

Philip Blumenfeld, BS,[1] Nobuhiko Hata, PhD,[1]* Simon DiMaio, PhD,[1] Kelly Zou, PhD,[1] Steven Haker, PhD,[1] Gabor Fichtinger, PhD,[2] and Clare M.C. Tempany, MD[1]

Purpose: To quantify needle placement accuracy of magnetic resonance image (MRI)-guided core needle biopsy of the prostate.

Materials and Methods: A total of 10 biopsies were performed with 18-gauge (G) core biopsy needle via a percutaneous transperineal approach. Needle placement error was assessed by comparing the coordinates of preplanned targets with the needle tip measured from the intraprocedural coherent gradient echo images. The source of these errors was subsequently investigated by measuring displacement caused by needle deflection and needle susceptibility artifact shift in controlled phantom studies. Needle placement error due to misalignment of the needle template guide was also evaluated.

Results: The mean and standard deviation (SD) of errors in targeted biopsies was 6.5 ± 3.5 mm. Phantom experiments showed significant placement error due to needle deflection with a needle with an asymmetrically beveled tip (3.2–8.7 mm depending on tissue type) but significantly smaller error with a symmetrical bevel (0.6–1.1 mm). Needle susceptibility artifacts observed a shift of 1.6 ± 0.4 mm from the true needle axis. Misalignment of the needle template guide contributed an error of 1.5 ± 0.3 mm.

Conclusion: Needle placement error was clinically significant in MRI-guided biopsy for diagnosis of prostate cancer. Needle placement error due to needle deflection was the most significant cause of error, especially for needles with an asymmetrical bevel.

Key Words: intraoperative MRI; biopsy; prostate; needle misplacement; accuracy assessment
J. Magn. Reson. Imaging 2007;26:688–694.

PROSTATE CANCER, the second most common cancer in men in the United States, is currently diagnosed by transrectal ultrasound (TRUS)-guided biopsy procedures (1). TRUS-guided biopsies are performed after test results indicate a high level of prostate-specific antigen (PSA) or abnormalities in a digital rectal exam (2). With ultrasound used as a guidance tool, six to 18 prostate tissue samples are typically acquired with a core biopsy needle. These core samples are removed from the apex, middle, and base of the left and right sides of the prostate gland to determine a diagnosis for cancer based on histological analysis. The overall sensitivity for sextant biopsies varies in the literature but is in the range of 60% to 85% (3–5). The positive predictive value for the tests varied as a function of patient and disease characteristics (4).

Magnetic resonance image (MRI)-guided prostate biopsy provides an alternative approach to detection and diagnosis of prostate cancer (6–8). MRI clearly delineates the prostate and its substructures, including the peripheral zone (PZ), the most common location of the cancer (9). The excellent imaging capabilities of MRI permit visualization of the sampling sites for sextant biopsies in the PZ (10). Furthermore, the ability of MRI to distinguish soft tissue allows classification of suspicious lesions and facilitates targeted biopsy of suspected tumor foci visible in the images. An additional advantage of interventional MRI guidance in obtaining biopsies is the ability to localize the biopsy needle by its artifact in coherent gradient echo images, allowing the radiologist to place the needle tip more precisely at a preplanned tissue site. MRI can also help to visualize tissue deformations within the prostate and the surrounding tissue during a biopsy procedure.

A recent study of 53 transperineal prostate biopsies, based on an approach that employs a 0.5-Tesla (T) open-configuration scanner and integrated navigation software (8), reported that MRI-guided targeted biopsy

[1]Department of Radiology, Brigham and Women's Hospital and Harvard Medical School, Boston, Massachusetts, USA.
[2]Engineering Research Center for Computer-Integrated Surgical Systems and Technologies (CISST), Johns Hopkins University, Baltimore, Maryland, USA.

Contract grant sponsor: Grosvenor Foundation; Contract grant sponsor: National Institutes of Health (NIH); Contract grant numbers: 1R01CA111288, 5R01EB002963, 5R01EB002963, 5P01CA067165, 5U41RR019703; Contract grant sponsor: National Science Foundation (NSF); Contract grant number: EEC 9731748.
The contents of this article are solely the responsibility of the authors and do not necessarily represent the official views of the NIH.

*Address reprint requests to: N.H., Department of Radiology, Brigham and Women's Hospital, 75 Francis St., Boston, MA 02115.
E-mail: hata@bwh.harvard.edu

Received June 15, 2006; Accepted June 1, 2007.
DOI 10.1002/jmri.21067
Published online in Wiley InterScience (www.interscience.wiley.com).

is a useful adjunct in the diagnosis of prostate cancer in patients with multiple negative TRUS biopsy results (11). The biopsies targeted at suspected tumor foci, observed in 1.5-T and/or 0.5-T preprocedural images, were of particular merit (11).

Although the transperineal MRI-guided prostate biopsy has improved the efficacy of prostate diagnosis through higher detection yields at targeted foci, the accuracy of core biopsy needle placement in transperineal procedures has not been evaluated. The accuracy of needle placement is especially significant because MRI-guided biopsy enables the collection of tissues from suspected tumor foci visible in MRI (11). The purpose of this study was to assess the accuracy of needle placement during MRI-guided prostate biopsies and to develop a taxonomy of those factors that contribute to misplacement. This investigation will facilitate improvements in the quality of MRI-guided prostate biopsy.

MATERIALS AND METHODS

A retrospective study of clinical data was performed to determine the accuracy of needle placement during MRI-guided prostate biopsies and the extent of needle misplacement. In addition, the source of targeting errors was investigated by means of controlled phantom studies based on the hypothesis that needle misplacement is due to several factors, including needle deflection, template misalignment, and spatial shift in the needle susceptibility artifact observed in intraprocedural images.

Targeting Error Based on a Study of Clinical Cases

A total of 10 randomly selected MRI-guided prostate biopsy cases (patient age = 61.9 ± 4.7 years; average prostate volume = 75.0 cc) were reviewed retrospectively. Details of the procedure, which is performed with an open-configuration 0.5-T scanner (Signa SP/i; GE Healthcare Technologies, Waukesha, WI, USA) are described in detail in D'Amico et al (6). This study was approved by the institutional review board, and conformed consent was obtained from all patients. All patients had 1.5-T endorectal coil MRI and 0.5-T MRI exams. The latter was performed during the biopsy with the patient in lithotomy position under general anesthesia.

Each patient underwent targeted biopsies, as well as systematic biopsies referred to as nontargeted biopsies. In targeted biopsies, core samples were taken from tumor foci found in 0.5-T T2-weighted (T2-w) images. In nontargeted biopsies, core samples were taken from sextant locations in the PZ of the prostate visible in 0.5-T T2-w images. The patients also underwent additional sampling based on statistically optimized locations in the prostate (12): these are included in the nontargeted sampling.

Both targeted and nontargeted biopsies were planned 10 to 15 minutes before the procedure on the basis of 0.5-T T2-w fast spin-echo images (TR/TE = 5000 msec/120 msec; field of view [FOV] = 12 cm; slice thickness = 3 mm; matrix size = 256 × 192). We measured the distances between these preplanned biopsy locations and the tip of the needle susceptibility artifact observed in intraprocedural coherent gradient echo images (TR/TE = 24.5 msec/12.1 msec; FOV = 24 cm; section thickness = 5 mm; matrix size = 256 × 128) used for monitoring needle placement during the imaging. We used either MRI-compatible 18-gauge (G) core biopsy needles with a symmetrical bevel (E-Z-EM, Westbury, NY, USA), termed *symmetrical needles*, or needles with an asymmetrical bevel (US Biopsy, Franklin, IN, USA), termed *asymmetrical needles*.

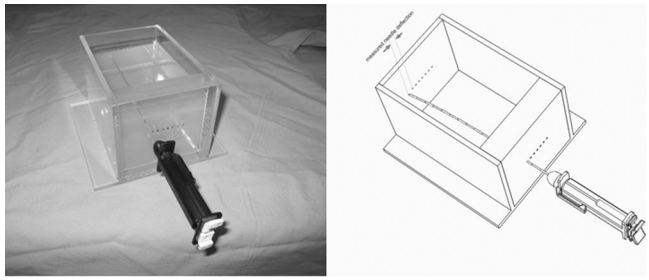

Figure 1. (left) Phantom and 18-G MRI-compatible needle (E-Z-EM, Westbury, NY, USA) for needle deflection analysis. Needle holes replicating the dimensions of the template guide used in MRI-guided prostate biopsy were prepared in one side of the acrylic enclosure with seven target points in the other side. (right) Schematic demonstrating the measurement of the needle deflection during phantom experiments.

We made our distance measurements without the depth discrepancy because our preliminary analysis indicated that the true depth of the needle tip is often misrepresented if the needle is out of the plane in the single-slice coronal or sagittal images used in clinical applications, thus limiting the accuracy of our measurements. Similar studies of transrectal prostate and breast biopsies have excluded the measurement of needle depth for the same reason (13,14).

For our analysis, the needle position was measured from the intraprocedural coherent gradient echo images with the display and mouse pointer attached to the MR scanner console. Results were tabulated and analyzed.

Effect of Needle Deflection in Phantom Experiments

Previous studies have shown that needle deflection is a significant source of error in needle placement (15,16). We therefore designed a phantom experiment to quantify this error. The phantom was constructed from an acrylic plastic enclosure with seven needle entry holes drilled through one side, aligned with seven target points on the opposite side (Fig. 1). The needle entry holes were 1.6 mm in diameter and 25.4 mm long, thereby replicating the dimensions of the template guide used to guide the needles during the MRI-guided prostate procedures at our institution. The interior distance between the two sides of the box was 120 mm. Samples of gelatin, bovine liver, and bovine muscle tissue were in turn placed inside the phantom enclosure. Needles were inserted through the entry holes and

phantom samples toward the marked target points at the distal end of the enclosure. We used the same MRI-compatible 18-G symmetrical and asymmetrical needles used in our clinical studies.

Both the symmetrical and asymmetrical needles were inserted seven times into each of the three different samples (gelatin and bovine liver and bovine muscle tissue), while two readers used a Vernier caliper to measure the resulting distance between the target point and the needle tip, observed visually through the clear plastic enclosure, thus measuring needle deflection (Fig. 1). Measurements of deflection for the asymmetrical needle were taken for both right and left orientations of the bevel. Results were tabulated and analyzed by statistical methods described below in Statistical Analysis.

Effect of Inaccurate Template Registration in Phantom Experiments

In MRI-guided transperineal biopsy, a needle-guidance grid, or template, is used to introduce the needles or template, with the patient in the lithotomy position. This template guide contains a grid of holes used for needle placement and is registered to the MRI coordinate frame by an optical tracking system (Flashpoint 5000; Image Guided Technologies, Boulder, CO, USA) that is integrated with the MRI scanner. This registration is used to compute the hole—and thus the needle trajectory—corresponding to each anatomical target determined from images taken immediately before the procedure. The tracking system is precalibrated to return coordinates in the scanner coordinate system and is used to measure the locations of four optical fiducial markers on the template. A rigid transformation is computed to bring the known template fiducial geometry into optimal alignment with these measured locations. The optimal transformation minimizes the sum of the squared error between the measured locations and the template fiducial points. The algorithm (17) was implemented with the Matlab mathematics software tool kit (Mathworks, Natick, MA, USA).

During template registration, errors can occur in the measurement of the template's fiducial point locations, thereby contributing to the targeting inaccuracy. To simulate the sensitivity of template registration to these errors, we analyzed fiducial coordinates acquired during four randomly selected clinical cases from the present study. In each case, the registration was computed with all combinations of only the fiducial coordinates—a leave-one-out strategy. The resulting variation in the calculated target locations caused by the variation in registration transformations, was analyzed by computing the target registration error (TRE), defined by Fitzpatrick et al (18). The four clinical cases had 22, 10, eight, and eight targets, respectively. Recomputed target coordinates were compared with the coordinates obtained from T2-w fast spin-echo images (TR/TE = 5000 msec/120 msec; FOV = 12 cm; slice thickness = 3 mm/0 mm gap; matrix size = 256 × 192), taken as ground truth.

Effect of Spatially-Shifted Needle Imaging Artifacts in Phantom Experiments

Needles composed of paramagnetic materials produce susceptibility artifacts that appear as regions of signal loss in MR images. The size, shape, and position of these artifacts depend on a number of factors, including imaging parameters, materials, and needle orientations. In general, such artifacts are spatially shifted along the frequency encoding direction, such that the observed image void is not aligned with the true needle location (19). We quantified this artifact shift in images acquired with the 0.5-T open-configuration MRI scanner (Signa SP/i; GE Healthcare, Waukesha, WI, USA) under imaging conditions identical to those used in the clinical MRI-guided biopsies described in D'Amico et al (6). Needles were scanned while they were immersed in water containing a gadolinium contrast agent (gadopentetate dimeglumine [Gd-DTPA]; Berlex Magnevist) at a ratio of 500:1. The needles were mounted to an acrylic plastic needle holder that also contained embedded fiducial markers with a known position relative to the needle shaft (Fig. 1). The Gd-DTPA was used to decrease the T1 relaxation time to increase the MR signal and produce a more homogeneous image around the needle. The phantom was placed in the 0.5-T open-configuration scanner, with the needle oriented perpendicularly to the static field (B_0) of the magnet, as is the case during clinical performance of prostate biopsies in which the patient is in the lithotomy position and the needle is inserted parallel to the superior-to-inferior (S/I) axis. coherent gradient echo images (TR/TE = 24.5 msec/12.1 msec; FOV = 24 cm; thickness = 5 mm; matrix size = 256 × 128) were acquired.

The experiment was repeated for different frequency encoding directions (right/left and anterior/posterior) and slice thickness (5 mm and 7 mm). Established clinical practice dictated the choice of these variables. A total of 19 transverse images were taken for each combination of the parameters, and the differences between the actual positions of the needles and the centers of the artifacts were measured.

Statistical Analysis

The errors in the clinical studies were summarized using mean, standard deviation (SD), and median values, stratified by location and by target vs. nontarget. Outliers were excluded when the z-score of the error was more than ±3, where the z-score is defined as (data mean)/(SD) within each case. This analysis was conducted with the Microsoft Excel 2003 Analysis Toolpak with the data analysis add-in. By convention, the statistical significance was defined as $P \leq 0.05$.

The errors of the last three phantom studies were summarized from their mean errors and SD. Statistical differences of errors in targeted and nontargeted biopsies and among three tissue types in the needle deflection analysis were assessed by two-sided paired Student's *t*-test. By convention, the statistical significance was defined as $P \leq 0.05$.

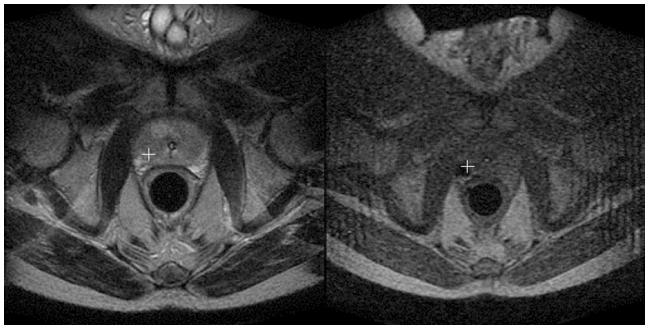

Figure 2. Representative MR images from a clinical study (64 years old; PSA = 18.0 ng/dL; prostate volume = 67.6 cc). A preprocedural T2-w image with the target (white cross mark) (left) and intraprocedural coherent gradient echo image from the same study targeting the same target (white cross mark) (right). The needle artifact in the coherent gradient echo images indicates needle location.

RESULTS

The mean and SD of the errors in targeted biopsies was 6.5 ±3.5 mm, with a median of 6.4 mm, while for nontargeted locations, the mean error was 6.7 ± 4.4 mm, with a median of 6.0 mm. The difference in the mean errors between the targeted biopsy and nontargeted biopsy groups was statistically significant ($P < 0.001$). A representative axial MR image from the study is presented in Figs. 2, 3, and 4.

The results from all the phantom experiments, including the mean tip deflection and SD measured using the asymmetrical and symmetrical needles, can be viewed in Table 1. A relatively small correlation was found among different tissue types in trials with the symmetric needle ($P = 0.23$) as compared with trials with the asymmetric needle ($P < 0.0001$). The deflection with the asymmetrical needle was significantly greater than that with the symmetrical needle in all tissue samples.

The analysis of template registration yielded a mean targeting error of 1.5 ± 0.3 mm over 48 targeted sampling locations because of errors in template localization. The difference was significant for each case ($P <$ 0.001), each of which had a different number of biopsy targets (Table 2).

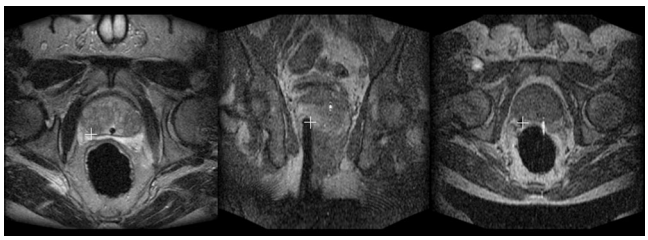

Figure 3. MR images from a clinical study (63 years old; PSA = 27.9 ng/dL; prostate volume = 116.0 cc) showing the deflection of needle in a targeted prostate biopsy. (left) T2-w image with cross mark indicating a target, (middle) coronal coherent gradient echo image with needle artifact and original tumor target location (cross mark), and (right) axial coherent gradient echo image with needle artifact and target location (cross mark). Note that the needle deflects toward the right side of the patient.

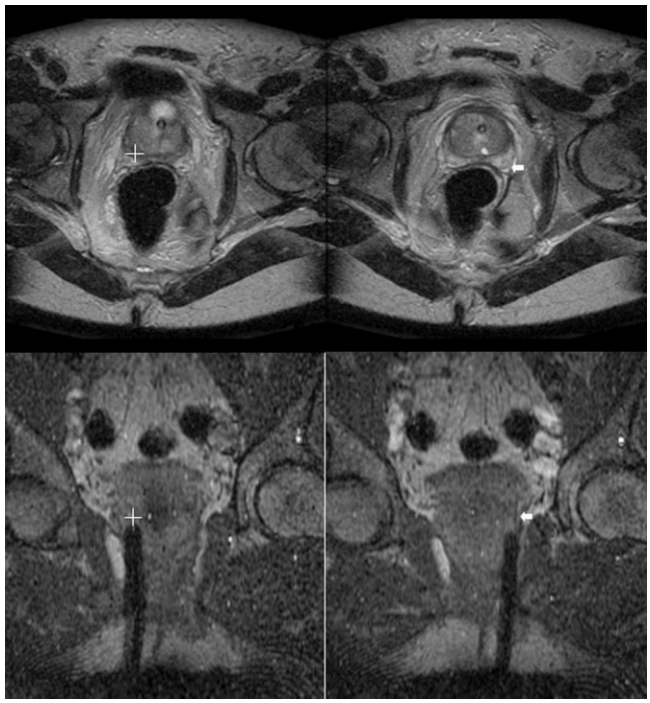

Figure 4. Representative MR images from clinical studies (60 years old; PSA = 8.3 ng/dL; prostate volume = 19.0 cc). Images on the top row are preprocedural T2-w images of (top left) tumor target site near the right lateral base (cross mark) and (top right) a sextant-sampling site at the left lateral base of the prostate (arrow). Images on the bottom row indicate typical needle angling with slight deflection visible in coronal coherent gradient echo images. In particular, the bottom left image shows the needle advancing toward the tumor target site near the right lateral base (cross mark) and the bottom right image shows the needle advancing toward the sextant target in the left lateral base (arrow).

The analysis of needle susceptibility artifact yielded a mean artifact shift of 1.6 ±0.4 mm along the direction of the frequency encoding direction (Table 3).

DISCUSSION

In conclusion, we have shown that the needle placement accuracy of transperineal biopsy of prostate cancer in open-configuration 0.5-T MRI is 6.5 mm and that needle deflection is the primary source of error, particularly when an asymmetrical tip bevel is used in the current method of needle placement with a template guide. Ideally, we should be able to target prostatic malignances that one visually identifies in the guidance image. In other words, we require that there be no loss of sensitivity due to technical imperfections. A recent study by Nakashima et al (20) suggests that endorectal MRI is useful for predicting local extension, as well as tumor site and tumor size, of cancer foci greater than 10 mm in diameter, while MRI did not correlate significantly with the histological diameter of tumors smaller than 10 mm. Using magnetic resonance spectroscopy imaging (MRSI), regions of absent or low citrate concen-

Table 1
Error Due to Needle Deflection

Error due to	Phantom setup	Mean error (mm)	SD (mm)	Correlation
Asymmetrical needle deflection	Gelatin	4.6	0.4	$P < 0.001$
	Bovine liver	3.2	0.5	
	Bovine muscle tissue	8.7	0.8	
Symmetrical needle deflection	Gelatin	0.8	0.6	$P = 0.23$
	Bovine liver	0.6	0.6	
	Bovine muscle tissue	1.1	0.5	

tration in the prostate can be visualized at a resolution of a few millimeters (21); however, there has been no strong evidence that a single positive voxel would indeed indicate malignancy. Nevertheless, expecting future improvements in both MRI and MRSI target identification, we aim to achieve 3.0-mm needle placement accuracy.

The three different phantom materials demonstrated the effect of tissue properties on deflection. Although MRI guidance enables a targeted prostate biopsy approach, our clinical study indicated that the method is limited by the accuracy of needle placement and that a number of physical factors are significant sources of placement error, some of which were demonstrated in our phantom study. These findings agreed with those of Okamura et al (22) on force modeling for needle insertion into soft tissue, which showed that a beveled tip causes more needle bending and is more easily affected by variations in tissue density.

We also found that template registration error and spatial shifts in the susceptibility artifacts contribute an average of 1.5 mm and 1.6 mm to systematic error, respectively. While imaging artifacts do not affect placement accuracy directly, they can influence visualization of the needle position and hence the accuracy of needles repositioned on the basis of this feedback. Several studies on needle artifact in MRI-guided biopsy have been published (23–27). It is now known that frequency encoding parallel to the needle distorts the image along the needle, that frequency encoding perpendicular to the needle distorts the image perpendicular to the needle, and that a needle placed parallel to B_0 minimizes the width of the needle artifact (25). In our clinical application of MR-guided prostate biopsy, patients in the lithotomy position lie perpendicular to the B_0 direction, placing the needle perpendicular to the B_0 direction and thus widening the artifact. This widening is exacerbated by the coherent gradient echo imaging sequence, which is known to produce larger needle artifacts than either fast spin-echo or turbo spin-echo sequences. Therefore, a weakness of our clinical study is the measurement inaccuracy caused by the difficulty of precisely distinguishing the center of the needle from the artifact. The relatively large discrepancy between variance in phantom studies and clinical studies may be due to this difficult. Our clinical study of 10 cases demonstrated a higher inaccuracy in targeted biopsies (6.5 mm) than in other accuracy studies of MRI-guided biopsies, and the cause of this difference needs to be discussed and investigated further.

Although we did not investigate this in our phantom experiments, the use of a fixed needle template guide with holes spaced 5 mm apart also significantly limits the resolution of needle placement and constrains needle orientation.

Other groups have reported other forms of prostate biopsy under MRI guidance. Zangos et al (7) reported a transgluteal approach with a 0.2-T MRI system, in which a median of 3.8 samples were obtained with a 15-G pencil tip with a 16-G biopsy handy from the prostate gland, guided by T1-weighted fast low-angle shot (FLASH) sequence images; however, they did not specifically target the tumor foci. Beyersdorff et al (2) reported 12 cases of targeted biopsies in a 1.5-T MR unit with a specially designed needle-guidance device using a transrectal approach.

Krieger et al (28) demonstrated remotely navigated placement of a transrectal marker seed and biopsy inside high-field closed MRI scanners. They reported good accuracy with a fast actuation gun and a transrectal access route that together could effectively mitigate the extent of tissue dislocation and deformation. At the same time, this transrectal approach samples the PZ across its smallest dimension and is hence more prone to missing the cancer than is the transperineal approach. Furthermore, some locations in the prostate were not accessible because they were blocked by the urethra. Also important, the transrectal technique is not extendible to brachytherapy and other local therapy options that require many needle placements because of increased rectal injury and thereby a higher risk of infection.

Table 2
Targeting Error Due to Template Registration

Case no.	No. of cores	MR sites	Mean (mm)	SD (mm)
1	22	Right mid, right base, right Apex	1.5	0.2
2	10	Left base, left mid	1.4	0.1
3	8	Right base	1.5	0.2
4	8	Right mid	1.9	0.3

Table 3
Error Due to Artifact Susceptibility

Phantom setup	Mean error (mm)	SD (mm)
Gadolinium; 5-mm slice; R/L frequency	1.6	0.1
Gadolinium; 5-mm slice; A/P frequency	1.8	0.2
Gadolinium; 7-mm slice; R/L frequency	1.7	0.4
Gadolinium; 7-mm slice; A/P frequency	1.4	0.5

R/L = right-to-left, A/P = anterior-to-posterior.

Susil et al (13) also tested accuracy using data from four procedures in which 32 targeted biopsy needles were placed within the prostate. They reported a mean needle-placement accuracy of 2.1 mm, with 95% of biopsies taken within 4.0 mm of their targets and a maximum of 4.4 mm (13). They used 14-G needles, in which case needle deflection was minimal, but tissue deformation and dislocation must have been pronounced. Also, they moved the patient out of the bore for needle insertions and then returned the patient into the bore to confirm satisfactory placement of the needle. However, they did not take superior-inferior (depth) error into account because they claimed that inaccuracy due to this error was minimal and not as significant as the transverse error. Moreover, the paired Student's *t*-test showed superior-inferior discrepancy to be significantly higher than the right/left or anterior/posterior discrepancy at the target locations.

This study also relates to a previous accuracy study in MR-guided biopsy of breast (14). Using an apparatus that stabilized the breast, Schneider et al (14) reported mean spatial accuracy of needle placement from the center of the targeted lesions. For a 20-G needle (N = 13) the error was 1.2 ±1.4 mm, whereas for a 14-G needle, the mean accuracy was 5.6 mm (N = 2). They reported that the mechanical spacing of the rectilinear grid of holes in the needle guide was the major contribution to the error. However, our study shows that, depending on the type of needle and its insertion depth, needle deflection can also be a major cause of error in prostate biopsies. Thus, we conjecture that a mechanism that provides more accurate and flexible needle placement than do contemporary stereotactic template guides as well as real-time imaging during needle insertion would increase the accuracy of MR-guided prostate biopsy significantly. To this end, we have designed a comprehensive robotic assistant system to perform prostate biopsy and brachytherapy procedures entirely inside a 3-T closed MRI scanner (16).

In summary, we have analyzed needle placement errors in MRI-guided biopsies of prostate cancer in a retrospective clinical study and a phantom study. We showed a mean error of 6.5 mm from 10 clinical cases for targeted biopsies. Phantom experiments showed that needle placement error due to needle deflection was significant when a needle with asymmetrical bevel was used; the inaccuracies in needle placement due to needle artifact susceptibility and template registration were a nominal 1.5 mm and 1.6 mm, respectively, leading us to believe that one cause of significant placement error, 6.5 mm, in clinical practice is needle deflection. Our study was at a slight disadvantage due to the low field strength. Future accuracy studies should be performed using a 1.5-T MR system. Although this may introduce new errors, the better field strength will give a better image quality and may improve the current accuracy of prostate biopsies under MR. Additional factors also need to be assessed further.

ACKNOWLEDGMENTS

We thank Ms. Janice Fairhurst and Mr. Daniel Kacher of Brigham and Women's Hospital for their technical support, and Ms. Angela Roddy Kanan for her clinical support. P.B. was supported by the Grosvenor Foundation.

REFERENCES

1. Weir HK, Thun MJ, Hankey BF, et al. Annual report to the nation on the status of cancer, 1975–2000, featuring the uses of surveillance data for cancer prevention and control. J Natl Cancer Inst 2003; 95:1276–1299.
2. Beyersdorff D, Winkel A, Hamm B, Lenk S, Loening SA, Taupitz M. MR imaging-guided prostate biopsy with a closed MR unit at 1.5 T: initial results. Radiology 2005;234:576–581.
3. Terris MK. Sensitivity and specificity of sextant biopsies in the detection of prostate cancer: preliminary report. Urology 1999;54: 486–489.
4. Mettlin C, Lee F, Drago J, Murphy GP. The American-Cancer-Society National Prostate-Cancer detection project—findings on the detection of early prostate cancer in 2425 men. Cancer 1991;67: 2949–2958.
5. Norberg M, Egevad L, Holmberg L, Sparen P, Norlen BJ, Busch C. The sextant protocol for ultrasound-guided core biopsies of the prostate underestimates the presence of cancer. Urology 1997;50: 562–566.
6. D'Amico AV, Tempany CM, Cormack R, et al. Transperineal magnetic resonance image guided prostate biopsy. J Urol 2000;164: 385–387.
7. Zangos S, Eichler K, Engelmann K, et al. MR-guided transgluteal biopsies with an open low-field system in patients with clinically suspected prostate cancer: technique and preliminary results. Eur Radiol 2005;15:174–182.
8. Hata N, Jinzaki M, Kacher D, et al. MR imaging-guided prostate biopsy with surgical navigation software: device validation and feasibility. Radiology 2001;220:263–268.
9. Adusumilli S, Pretorius ES. Magnetic resonance imaging of prostate cancer. Semin Urol Oncol 2002;20:192–210.
10. Wefer AE, Hricak H, Vigneron DB, et al. Sextant localization of prostate cancer: comparison of sextant biopsy, magnetic resonance imaging and magnetic resonance spectroscopic imaging with step section histology. J Urol 2000;164:400–404.
11. So MJ, Haker S, Zou KH, et al. Clinical evaluation of MR-guided prostate biopsy. In: Proceedings of the 13th Annual Meeting of ISMRM, Miami Beach, FL, USA, 2005 (Abstract 264).
12. Shen D, Lao Z, Zeng J, et al. Optimized prostate biopsy via a statistical atlas of cancer spatial distribution. Med Image Anal 2004;8:139–150.
13. Susil RC, Camphausen K, Choyke P, et al. System for prostate brachytherapy and biopsy in a standard 1.5 T MRI scanner. Magn Reson Med 2004;52:683–687.
14. Schneider E, Rohling KW, Schnall MD, Giaquinto RO, Morris EA, Ballon D. An apparatus for MR-guided breast lesion localization and core biopsy: design and preliminary results. J Magn Reson Imaging 2001;14:243–253.
15. DiMaio SP, Salcudean SE. Interactive simulation of needle insertion models. IEEE Trans Biomed Eng 2005;52:1167–1179.
16. DiMaio SP, Salcudean SE. Needle steering and motion planning in soft tissues. IEEE Trans Biomed Eng 2005;52:965–974.
17. Horn BKP, Hilden HM, Negahdaripour S. Closed form solution of absolute orientation using orthonormal matrices. J Optical Soc A 1988;4:51127–51135.
18. Fitzpatrick JM, West JB, Maurer CR Jr. Predicting error in rigid-body point-based registration. IEEE Trans Med Imaging 1998;17: 694–702.

19. Schenck JF. The role of magnetic susceptibility in magnetic resonance imaging: MRI magnetic compatibility of the first and second kinds. Med Phys 1996;23:815–850.
20. Nakashima J, Tanimoto A, Imai Y, et al. Endorectal MRI for prediction of tumor site, tumor size, and local extension of prostate cancer. Urology. 2004;64:101–105.
21. Wu X, Dibiase SJ, Gullapalli R, Yu CX. Deformable image registration for the use of magnetic resonance spectroscopy in prostate treatment planning. Int J Radiat Oncol Biol Phys 2004;58:1577–1583.
22. Okamura AM, Simone C, O'Leary MD. Force modeling for needle insertion into soft tissue. IEEE Trans Biomed Eng 2004;51:1707–1716.
23. Butts K, Pauly JM, Daniel BL, Kee S, Norbash AM. Management of biopsy needle artifacts: techniques for RF-refocused MRI. J Magn Reson Imaging 1999;9:586–595.
24. Lewin JS, Duerk JL, Jain VR, Petersilge CA, Chao CP, Haaga JR. Needle localization in MR-guided biopsy and aspiration: effects of field strength, sequence design, and magnetic field orientation. AJR Am J Roentgenol 1996;166:1337–1345.
25. Ladd ME, Erhart P, Debatin JF, Romanowski BJ, Boesiger P, McKinnon GC. Biopsy needle susceptibility artifacts. Magn Reson Med 1996;36:646–651.
26. Liu H, Martin AJ, Truwit CL. Interventional MRI at high-field (1.5 T): needle artifacts. J Magn Reson Imaging 1998;8:214–219.
27. Liu H, Hall WA, Martin AJ, Truwit CL. Biopsy needle tip artifact in MR-guided neurosurgery. J Magn Reson Imaging 2001;13:16–22.
28. Krieger A, Susil RC, Menard C, et al. Design of a novel MRI compatible manipulator for image guided prostate intervention. IEEE Trans Biomed Eng 2005;52:306–313.